

Three Dimensional T-Ray Inspection Systems

by

Bradley Ferguson

B.E. (Electrical & Electronic, First Class Honours),
The University of Adelaide, Australia, 1997

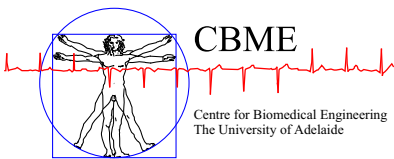
Thesis submitted for the degree of

Doctor of Philosophy

in

School of Electrical and Electronic Engineering,
Faculty of Engineering, Computer and Mathematical Sciences
The University of Adelaide, Australia

December, 2004



© 2004
Bradley Ferguson
All Rights Reserved



Contents

Heading	Page
Contents	iii
Abstract	ix
Statement of Originality	xi
Acknowledgments	xiii
Thesis Conventions	xv
Publications	xvii
List of Figures	xxi
List of Tables	xxix
Chapter 1. Introduction and Motivation	1
1.1 Introduction	2
1.1.1 THz Radiation	2
1.2 Background	3
1.2.1 The Electromagnetic Spectrum	3
1.2.2 THz Spectroscopy Systems	3
1.3 Motivation	6
1.3.1 Three Dimensional THz Imaging Systems	6
1.3.2 THz Inspection Systems	8
1.4 Thesis Overview	8
1.5 Original Contributions	11
Chapter 2. Historical Landscape	13
2.1 THz Sources	14

2.1.1	Broadband THz Sources	14
2.1.2	Narrowband THz Sources	16
2.2	THz Detectors	20
2.3	THz Applications	23
2.3.1	Material Characterisation	23
2.3.2	THz Imaging	24
2.3.3	Biomaterial THz Applications	26
2.4	Outlook	28
Chapter 3. THz Imaging		29
3.1	Introduction	30
3.1.1	Passive THz Imaging	30
3.1.2	Active THz Imaging	34
3.2	THz Imaging Horizons and Hurdles	35
3.2.1	Horizons and Goals	35
3.2.2	Challenges and Hurdles	36
3.3	Pulsed THz Imaging Architectures	44
3.3.1	Traditional Scanning THz Imaging	45
3.3.2	Two Dimensional Free Space EO Sampling	51
3.3.3	THz Imaging with a Chirped Probe Pulse	63
3.3.4	Other THz Imaging Methods	73
3.4	Chapter Summary	74
Chapter 4. Three dimensional THz Imaging		77
4.1	Introduction	78
4.2	Review of Tomography Techniques	79
4.2.1	X-ray Tomography	79
4.2.2	Optical Tomography	80
4.2.3	RF Tomography	82
4.2.4	Ultrasound Tomography	83
4.3	Review of THz Tomography Techniques	83

4.3.1	Tomography with a Fresnel Lens	83
4.3.2	Time Reversal Imaging	87
4.3.3	Multistatic Imaging	89
4.4	T-ray Holography	92
4.4.1	Introduction	92
4.4.2	2D T-ray Holography	93
4.4.3	3D T-ray Holography	101
4.4.4	Windowed Fourier Transform	104
4.4.5	Reconstruction Algorithm	105
4.4.6	Experimental Results	107
4.4.7	Summary	109
4.5	T-ray Diffraction Tomography	109
4.5.1	Wave Propagation Theory	109
4.5.2	T-ray Diffraction Tomography System	113
4.5.3	Reconstruction Algorithm	115
4.5.4	Experimental Results	119
4.5.5	Summary	128
4.6	T-ray Computed Tomography	129
4.6.1	Introduction	129
4.6.2	X-ray Tomography	129
4.6.3	T-ray CT Reconstruction Algorithm	133
4.6.4	T-ray CT Optical Design	138
4.6.5	2D T-ray CT	140
4.6.6	3D T-ray Computed Tomography	163
4.6.7	Amplitude vs Phase Reconstructions	172
4.7	Chapter Summary	178
4.7.1	T-ray Holography	179
4.7.2	T-ray DT	179
4.7.3	T-ray CT	180
4.7.4	Looking Forward	180

Chapter 5. Material Identification Using THz Imaging	183
5.1 Introduction	184
5.1.1 Pattern Recognition	184
5.1.2 THz Classification	187
5.2 Preprocessing	188
5.2.1 Definitions and Notation	191
5.2.2 Problem Definition	191
5.2.3 Wavelet Denoising	192
5.2.4 Deconvolution	201
5.2.5 Comparison of Techniques	204
5.2.6 Conclusion	206
5.3 Feature Extraction	208
5.3.1 The Curse of Dimensionality	209
5.3.2 System Identification Filter Coefficients	209
5.3.3 Deconvolved Frequency Coefficients	212
5.4 Feature Selection	214
5.4.1 Statistical t-test	214
5.4.2 Classification Accuracy	216
5.4.3 Genetic Algorithms	216
5.5 Classification	220
5.5.1 Bayesian Classification	221
5.5.2 Mahalanobis Distance	222
5.5.3 Other Methods	223
5.6 Case Study #1: Tissue Identification	223
5.6.1 Data Acquisition	224
5.6.2 Linear Modelling	226
5.6.3 Classification	227
5.6.4 Conclusion	233
5.7 Case Study #2: Powder Detection	235
5.7.1 Data Acquisition	237

5.7.2	Classification	243
5.7.3	Conclusion	248
5.8	Case Study #3: Cancer Detection	249
5.8.1	Common Skin Cancer Indicators	250
5.8.2	Existing Techniques	251
5.8.3	Far-Infrared Techniques	252
5.8.4	Sample Preparation	254
5.8.5	Imaging Results	255
5.8.6	Cell Classification	258
5.8.7	Comparison with Principal Component Analysis	259
5.8.8	Conclusions and Future Directions	265
5.9	Chapter Summary	267
 Chapter 6. Conclusion		 269
6.1	Introduction	270
6.2	Thesis Summary	270
6.2.1	THz Imaging Systems	270
6.2.2	T-ray Tomography	272
6.2.3	Material Identification	276
6.3	Future Directions	278
6.4	Summary of Original Contributions	281
6.5	In Closing	283
 Appendix A. Hardware Specifications		 285
 Appendix B. Software Implementation		 289
B.1	MFCPentaMax	289
B.2	Labview Tomography Application	289
B.3	Slicer Dicer	290
B.4	Matlab Code	291
B.4.1	Code Listings	292

Contents

Appendix C. Refractive Index Extraction	339
C.1 Problem Geometry	339
Appendix D. Radon's Inversion Formula	343
D.1 Derivation	343
D.2 Practical Difficulties	345
Appendix E. The Curse of Dimensionality	347
Bibliography	349
Glossary	381
Index	383
Résumé	387

Abstract

Pulsed terahertz (THz) systems are an emergent technology, finding diverse applications as they approach maturity. From their birth in the late 1980's to the wealth of alternate sources and imaging modalities now available, the rise has been fuelled by the expectation that this will prove a world changing technology. This Thesis takes an application focused approach and seeks to provide enabling systems and algorithms for the development of *functional* imaging systems with broad potential application in security inspection, non-destructive testing and biomedical imaging.

Three dimensional pulsed THz imaging systems were first introduced in 1996 using a reflection-mode ultrasound-like configuration. This Thesis builds upon this former work by focusing on *transmission* mode tomography systems using pulsed THz radiation. Several novel 3D imaging modalities are introduced. The hardware architectures, based on optoelectronic generation and detection of THz radiation are described. Approximations to the wave equation are derived, allowing linear reconstruction algorithms to recover 3D structural information from the transmitted THz field. Finally the systems are demonstrated and the achievable resolution and image quality are investigated. Three imaging architectures are developed herein:

1. T-ray holography allows the 3D distribution of point scatters to be resolved based on a single projection image utilising a novel reconstruction algorithm based on the windowed Fourier transform and back-propagation of the Fresnel-Kirchhoff diffraction equation.
2. T-ray diffraction tomography utilises the diffracted THz field to allow a Helmholtz equation based, frequency-dependent reconstruction to be performed and the THz spectrum at each pixel to be calculated.
3. T-ray Computed Tomography (CT) uses analogous techniques to X-ray CT, based on the Radon transform, to provide 3D T-ray reconstructions of unprecedented fidelity.

These techniques have important applications in material identification, which is investigated in the second part of this Thesis.

Pulsed THz spectroscopy has been widely acclaimed for its potential to identify different materials based on their spectral properties. The second part of this Thesis presents algorithms towards this goal. Three case studies are performed focusing on biomaterial classification, anthrax detection and *in vitro* osteosarcoma cell differentiation. A classification framework is developed to process the THz spectral data and identify specific materials. A linear filter model is introduced to describe the system response of different materials, and the filter taps are utilised for feature extraction. This technique is demonstrated for biomaterial and anthrax classification. For cell differentiation a genetic algorithm is used to select deconvolved frequency components to train a classifier. In each case a high classification accuracy is demonstrated, highlighting the promise and potential of three dimensional T-ray inspection systems.

Statement of Originality

This work contains no material that has been accepted for the award of any other degree or diploma in any university or other tertiary institution and, to the best of my knowledge and belief, contains no material previously published written by another person, except where due reference has been made in the text.

I give consent to this copy of the thesis, when deposited in the University Library, being available for loan, photocopying and dissemination through the digital thesis collection.

A handwritten signature in black ink, appearing to read 'B. Ferguson'.

29th December, 2004

Signed

Date

Acknowledgments

A great number of people have collaborated to make this Ph.D. an exceptionally rewarding and memorable experience. I extend my sincerest thanks to my family, friends, colleagues and supervisors for their support and encouragement.

I thank my supervisor Associate Professor Derek Abbott for introducing me to the world of terahertz imaging and for the continuous flow of ideas that he provided. I also thank him for his encouragement and tireless work in reviewing journal publications and this Thesis. My co-supervisor Professor Doug Gray provided welcome advice and contributed significantly to the development of linear filter models for THz classification.

I had the pleasure of working with one of the true pioneers of THz imaging, Professor X.-C. Zhang (Rensselaer Polytechnic Institute, USA). I hold him in the highest esteem for captivating me with his vision of the potential of THz research and for his inspiration and guidance.

While a Ph.D. is, by nature, a solitary experience, I have benefitted greatly from interaction with colleagues at the University of Adelaide and at Rensselaer Polytechnic Institute. I wish to acknowledge Dr Samuel Mickan, Dr Greg Harmer, Leonard Hall, Hua Zhong, Haibo Liu and Jingqun Xi. A special debt of gratitude is also owed to Dr Shaohong Wang from Rensselaer Polytechnic Institute. Much of the work in this Thesis is a result of our fruitful collaboration.

Thanks are due to Matthew Berryman and Gretel M. Png for proof-reading this Thesis, and to Dr Greg Harmer for gracious provision of the L^AT_EX template. Thanks also to Dr David Findlay and Shelly Hay from the Royal Adelaide Hospital for supplying cancer cell samples for THz spectroscopy studies.

I thank my parents for their love and for teaching me that “... *the LORD gives wisdom, from His mouth come knowledge and understanding.*” – *Proverbs 2:6*. I also thank the rest of my family: Daniel, Cameron, Mark, Amanda and Rebecca, for memories and support.

I gratefully acknowledge the many funding agencies whose generous grants facilitated this research. This work was enabled by the Mutual Community Travel Award,

Acknowledgments

the D.R. Stranks Scholarship, the Optical Society of America and New Focus Award, the International Society for Optical Engineering, the AFUW, the SA Premier's Department and the Australian Research Council. This work was also supported in part by the Center for Subsurface Sensing and Imaging Systems, under the Engineering Research Centers Program of the National Science Foundation (award number EEC-9986821), and the Cooperative Research Centre for Sensor, Signal and Information Processing (CSSIP). Support was also provided by the University of Adelaide B3 medical funding scheme and the University of Adelaide Small Grants Funding Scheme. Special thanks are due to the Australian-American Fulbright Commission for funding and for the opportunity of a lifetime in the form of a two-year educational exchange to Rensselaer Polytechnic Institute in New York.

Finally, I owe everlasting gratitude to my wife Tennille, who has given me everything, at great cost, and with great love.

"Well, in our country," said Alice, still panting a little, "you'd generally get to somewhere else – if you ran very fast for a long time, as we've been doing."

"A slow sort of country!" said the Queen. "Now here, you see, it takes all the running you can do, to keep in the same place. If you want to get somewhere else, you must run at least twice as fast as that."

- Lewis Carroll (Carroll 1936)

"There are only two ways to live your life. One is as though nothing is a miracle. The other is as though everything is a miracle."

- Albert Einstein

Thesis Conventions

Typesetting. This Thesis is typeset using the L^AT_EX2e software. Processed plots and images were generated using Matlab 6.1 (Mathworks Inc.). CorelDRAW 8.4 (Corel Corporation) was used to produce schematic diagrams and other drawings. Pixotec Slicer Dicer (Pixotec Inc.) was used to generate 3D rendered images.

Spelling. Australian English spelling has been adopted throughout, as defined by the Macquarie English Dictionary (A. Delbridge, Ed., Macquarie Library, North Ryde, NSW, Australia, 2001). Where more than one spelling variant is permitted such as 'biassing' or 'biasing' and 'infra-red' or 'infrared' the option with the fewest characters has been chosen.

Referencing. The Harvard style is used for referencing and citation in this Thesis.

Publications

- FERGUSON-B., AND ABBOTT-D. (2000). Signal processing for T-ray bio-sensor systems, *Proc. SPIE - Smart Electronics and MEMS II*, Vol. 4236, Melbourne, Australia, pp. 157–169.
- FERGUSON-B., AND ABBOTT-D. (2001a). De-noising techniques for terahertz responses of biological samples, *Microelectronics Journal*, Elsevier, **32**(12), pp. 943–953.
- FERGUSON-B., AND ABBOTT-D. (2001b). Wavelet de-noising of optical terahertz pulse imaging data, *Journal of Fluctuation and Noise Letters*, **1**(2), pp. L65–L69.
- FERGUSON-B., AND ZHANG-X.-C. (2002a). Materials for terahertz science and technology, *Nature Materials*, **1**(1), pp. 26–33.
- FERGUSON-B., AND ZHANG-X.-C. (2002b). T-ray computed tomography, *Laser Focus World*, pp. 133–135.
- FERGUSON-B., AND ZHANG-X.-C. (2003a). THz science and technology, *WuLi (Physics)*, **32**, pp. 286–293.
- FERGUSON-B. S., LIU-H., HAY-S., FINDLAY-D., GRAY-D., ZHANG-X.-C., AND ABBOTT-D. (2003a). In vitro osteosarcoma biosensing using THz time domain spectroscopy, *Proc. SPIE - BioMEMS and Nanotechnology*, Vol. 5275, Perth, Australia, pp. 304–316.
- FERGUSON-B., MICKAN-S., HUBBARD-S., PAVLIDIS-D., AND ABBOTT-D. (2001a). Investigation of gallium nitride T-ray transmission characteristics, *Proc. SPIE - Electronics and Structures for MEMS II*, Vol. 4591, Adelaide, Australia, pp. 210–220.
- FERGUSON-B. S., WANG-S., ZHONG-H., ABBOTT-D., AND ZHANG-X.-C. (2003b). Powder retection with THz imaging, in R. J. Hwu and D. L. Woolard, (eds.), *Proc SPIE - Terahertz for Military and Security Applications*, Vol. 5070, Orlando, FL, pp. 7–16.
- FERGUSON-B., WANG-S., AND ZHANG-X. (2001b). T-ray computed tomography, *2001 IEEE/LEOS Annual Meeting Conference Proceedings*, IEEE, San Diego, pp. PD1.7–PD1.8.

- FERGUSON-B., WANG-S., GRAY-D. A., ABBOTT-D., AND ZHANG-X.-C. (2001c). Terahertz imaging of biological tissue using a chirped probe pulse, in N. W. Bergmann, (ed.), *Proc. SPIE - Electronics and Structures for MEMS II*, Vol. 4591, Adelaide, Australia, pp. 172–184.
- FERGUSON-B., WANG-S., GRAY-D., ABBOTT-D., AND ZHANG-X.-C. (2002a). T-ray computed tomography, *Optics Letters*, **27**(15), pp. 1312–1314.
- FERGUSON-B., WANG-S., GRAY-D., ABBOTT-D., AND ZHANG-X.-C. (2002b). T-ray diffraction tomography, *OSA Trends in Optics and Photonics (TOPS), The Thirteenth International Conference on Ultrafast Phenomena*, Vol. 72, Optical Society of America, Vancouver, pp. 450–451.
- FERGUSON-B., WANG-S., GRAY-D. A., ABBOTT-D., AND ZHANG-X.-C. (2002c). T-ray tomographic imaging, in D. V. Nicolau and A. P. Lee, (eds.), *Proc. SPIE - Biomedical Applications of Micro- and Nanoengineering*, Vol. 4937, Melbourne, Australia, pp. 62–72.
- FERGUSON-B., WANG-S., GRAY-D., ABBOTT-D., AND ZHANG-X.-C. (2002d). Three dimensional imaging using T-ray computed tomography, *OSA Trends in Optics and Photonics (TOPS), Proceedings of Conference on Lasers and Electro-Optics*, Vol. 73, Optical Society of America, Long Beach, CA, p. 131.
- FERGUSON-B., WANG-S., GRAY-D., ABBOTT-D., AND ZHANG-X.-C. (2002e). Towards functional 3D T-ray imaging, *Physics in Medicine and Biology*, **47**(21), pp. 3735–3742.
- FERGUSON-B., WANG-S., GRAY-D., ABBOTT-D., AND ZHANG-X.-C. (2002f). Identification of biological tissue using chirped probe THz imaging, *Microelectronics Journal*, Elsevier, **33**(12), pp. 1043–1051.
- FERGUSON-B., WANG-S., XI-J., GRAY-D., ABBOTT-D., AND ZHANG-X.-C. (2003c). Linearized inverse scattering for three dimensional terahertz imaging, *OSA Trends in Optics and Photonics (TOPS), Proceedings of Conference on Lasers and Electro-Optics*, Vol. 89, Optical Society of America, Baltimore, MD, p. CMP1.
- TE-C. C., FERGUSON-B., AND ABBOTT-D. (2002). Investigation of biomaterial classification using T-rays, *Proc. SPIE - Biomedical Applications of Micro- and Nanoengineering*, Vol. 4937, Melbourne, Australia, pp. 294–306.

- WALSBY-E. D., WANG-S., FERGUSON-B., XU-J., YUAN-T., BLAIKIE-R., AND ZHANG-X.-C. (2002a). THz Fresnel lenses, *OSA Trends in Optics and Photonics (TOPS) Vol. 72, The Thirteenth International Conference on Ultrafast Phenomena*, Optical Society of America, Vancouver, pp. 131–132.
- WALSBY-E. D., WANG-S., FERGUSON-B., XU-J., YUAN-T., BLAIKIE-R., DURBIN-S. M., CUMMING-D. R. S., AND ZHANG-X.-C. (2002b). Multilevel silicon diffractive optics for THz waves, *Journal of Vacuum Science and Technology B*, **20**, pp. 2780–2783.
- WANG-S., FERGUSON-B., ABBOTT-D., AND ZHANG-X.-C. (2003a). T-ray imaging and tomography, *Journal of Biological Physics*, **29**(2/3), pp. 247–256.
- WANG-S., FERGUSON-B., AND ZHANG-X.-C. (2004). Pulsed terahertz tomography, *Journal of Physics D: Applied Physics*, **37**, pp. R1–R36. (See also Erratum *Journal of Physics D: Applied Physics*, **37**, p. 964.)
- WANG-S., FERGUSON-B., MANNELLA-C., ABBOTT-D., AND ZHANG-X.-C. (2002). Powder detection using THz imaging, *OSA Trends in Optics and Photonics (TOPS), Proceedings of Conference on Lasers and Electro-Optics*, Vol. 73, Optical Society of America, Long Beach, CA, p. 132.
- WANG-S., FERGUSON-B., ZHANG-C. L., AND ZHANG-X.-C. (2003c). Terahertz computer tomography, *Acta-Physica-Sinica*, **52**(1), pp. 120–124.
- WANG-S., FERGUSON-B., ZHONG-H., AND ZHANG-X.-C. (2003e). Three-dimensional terahertz holography, *OSA Trends in Optics and Photonics (TOPS), Proceedings of Conference on Lasers and Electro-Optics*, Vol. 89, Optical Society of America, Baltimore, MD, p. CMP6.

List of Figures

Figure		Page
1.1	The electromagnetic spectrum	4
1.2	Illustration of a THz-TDS pump probe system	5
1.3	T-ray reflective tomography image of a floppy disk	7
1.4	An overview of the Thesis structure	9
<hr/>		
2.1	Illustration of optical rectification	15
2.2	Conduction band structure of a THz quantum cascade laser	19
2.3	Illustration of free space electro-optic sampling	21
2.4	A broadband THz pulse	22
2.5	Foam used to insulate space shuttle fuel tanks	25
2.6	THz image of an onion cell membrane	26
2.7	A biotin-avidin T-ray biosensor	28
<hr/>		
3.1	Spectrum of blackbody radiation at low temperatures	31
3.2	Spectrum of blackbody radiation at ambient temperatures	32
3.3	THz pulse measured after transmission through various types of clothing	33
3.4	Passive THz image of a man	33
3.5	Near-field THz imaging based on SNOM	38
3.6	Photo of a THz imaging system	43
3.7	THz image of a butane flame	45
3.8	Illustration of scanned THz imaging	47
3.9	Comparison of THz pulses generated by PCA and OR emitters	48
3.10	Hardware schematic for scanned THz imaging	50
3.11	THz response obtained using a scanned THz imaging system	51
3.12	Scanned THz image of an oak leaf	52

List of Figures

3.13	Illustration of all-optical 2D THz imaging	53
3.14	Crossed polariser EO sampling geometry	53
3.15	Schematic of terahertz imaging with dynamic subtraction	56
3.16	Schematic of 2D FSEOS terahertz imaging with synchronised dynamic subtraction	58
3.17	Control signals for synchronised dynamic subtraction	59
3.18	Processing stages applied to 2D FSEOS images	61
3.19	The geometry of a diffraction grating	64
3.20	THz pulses measured with scanned EO sampling and EO sampling with a chirped probe pulse	68
3.21	Schematic for chirped probe terahertz imaging	69
3.22	An optical image of the pressed butterfly sample	70
3.23	THz images of the pressed butterfly sample	71
3.24	THz and optical images of a leaf	72
3.25	Terahertz responses of different numbers of pieces of paper	73
3.26	Zoomed view of THz responses of different numbers of pieces of paper	73
<hr/>		
4.1	Profile of a multi-level Fresnel zone plate	84
4.2	Schematic illustration of tomographic imaging with a Fresnel lens	86
4.3	1D time reversal imaging setup	88
4.4	2D time reversal image of a 10 mm wide star pattern	89
4.5	The measurement geometry used for Kirchhoff migration imaging	90
4.6	Scale model (1:2,400) of a destroyer imaged using THz SAR	92
4.7	Schematic of Young's double slit experiment	95
4.8	THz diffraction pattern caused by Young's double slits	96
4.9	Time domain double slit interference pattern	97
4.10	Frequency domain double slit interference pattern	98
4.11	Variation of fringe separation with THz wavelength	98
4.12	Variation of peak intensity with target to sensor distance	100
4.13	Double slit profile reconstructed using Fresnel backpropagation	100

4.14	2D double slit image reconstructed using Fresnel backpropagation . . .	101
4.15	Experimental setup for three-dimensional terahertz digital holography .	102
4.16	The THz waveform measured at the centre of the ZnTe sensor	103
4.17	Wave front images of the diffracted THz wave along three horizontal lines across the ZnTe EO sensor	104
4.18	Schematic of simple holography target samples and their reconstructed holograms	107
4.19	Schematic of holography target samples and their reconstructed holo- grams	108
4.20	Hardware schematic for T-ray diffraction tomography	114
4.21	The Fourier Diffraction Theorem in two dimensions	116
4.22	The classical diffraction tomography measurement configuration	116
4.23	Illustration of interpolation for diffraction tomography	118
4.24	The geometry of the T-ray DT experiment	120
4.25	THz image of a thin polyethylene cylinder for a single projection angle .	121
4.26	Reconstructed cross-section of the polyethylene cylinder	121
4.27	A test structure imaged by the T-ray DT system	122
4.28	The geometry of the T-ray DT test structure	123
4.29	Reconstructed cross-section of the polyethylene cylinders	124
4.30	Phase of the scattered field $\phi_s(\mathbf{r})$ measured across the CCD	125
4.31	Reconstructed 3D image of the polyethylene cylinders	126
4.32	Reconstructed refractive index of the polyethylene cylinders	127
4.33	T-ray DT reconstruction performed at 3 different frequencies	127
4.34	An object, $o(x, z)$, and its projection, $p(\theta, l)$	131
4.35	The depth of focus of a Gaussian beam	134
4.36	Geometry of the T-ray CT collection optics	139
4.37	Simple polystyrene test target	142
4.38	Time domain THz response of a 17 mm thick slab of polystyrene	142
4.39	Frequency domain THz response of a 17 mm thick slab of polystyrene .	143
4.40	Real refractive index of polystyrene	143
4.41	Extinction coefficient of polystyrene	143

List of Figures

4.42	Time domain THz responses of the triangular cylinder	145
4.43	Amplitude sinogram for triangular target	146
4.44	Example of τ estimation using interpolated cross-correlation	148
4.45	Timing sinograms for the triangular target	151
4.46	Reconstructed cross-section of the triangular polystyrene target	152
4.47	3D visualisation of the reconstructed cross-section of the triangular polystyrene target	153
4.48	Polystyrene block with the letters 'THZ' drilled into it	153
4.49	Timing sinogram for the 'THZ' target	154
4.50	Reconstructed cross-section of the 'THZ' polystyrene target	155
4.51	Detailed polystyrene resolution test target	156
4.52	Reconstructed cross-section of the resolution test target	157
4.53	3D visualisation of the reconstructed cross-section of the resolution test structure	157
4.54	Top view of polystyrene resolution test target	158
4.55	Reconstructed refractive index along line A'-A in Fig. 4.54	159
4.56	Deconvolved phase as a function of frequency	160
4.57	Fourier phase sinograms for the resolution target	161
4.58	Reconstructed cross-sections using the Fourier phase	162
4.59	Reconstructed frequency dependent refractive index	162
4.60	Variation in reconstructed image quality with frequency	163
4.61	The coordinate system used for T-ray CT	165
4.62	Top view of a 0.6 mm thick polyethylene sheet folded into an 'S' shape	166
4.63	A time domain reconstruction of the sheet of polyethylene	166
4.64	A 3D reconstruction of the sheet of polyethylene	167
4.65	Amplitude (ρ) sinogram for the turkey femur	168
4.66	A section of turkey femur imaged with the T-ray CT system	169
4.67	Reconstructed 3D image of a turkey femur	169
4.68	A vial and plastic tube were used for testing the T-ray CT system	170
4.69	Reconstructed vial and plastic tube	171

4.70	A 3D image of the reconstructed vial and plastic tube	171
4.71	Frequency dependent reconstructions of the vial target	172
4.72	The frequency dependent refractive index of the plastic inner tube shown in Fig. 4.68	173
4.73	A hollow celluloid sphere imaged using T-ray CT	173
4.74	Reconstructed slices of the celluloid sphere using ρ	175
4.75	Reconstructed slices of the celluloid sphere using τ	176
4.76	An example geometry for T-ray CT	176
4.77	Reconstructed 3D image of a celluloid sphere	178

5.1	Conceptual segmentation of the pattern recognition problem	186
5.2	Terahertz responses measured with differing LIA time constants	190
5.3	Block diagram of the elements used to define the problem	192
5.4	Examples of different wavelet basis functions, ψ	195
5.5	Wavelet coefficients for a T-ray response using different wavelet basis functions	195
5.6	Results of wavelet denoising the T-ray response for a leaf	200
5.7	Variation in denoised SNR vs wavelet order M	201
5.8	Results of Wiener denoising the T-ray response for a leaf	202
5.9	Block diagram illustrating the process of Wiener deconvolution	203
5.10	Frequency spectrum for two pixels on a piece of Spanish ham ('Jamon Serrano')	205
5.11	Frequency spectrum of ham T-ray pulses after Wiener deconvolution	205
5.12	A comparison of T-ray images before and after various processing stages	206
5.13	Wavelet denoising of THz data measured with a short LIA time constant	207
5.14	Example of the three main genetic operators	218
5.15	Flow chart of a genetic algorithm for feature selection	219
5.16	Optical image of a section of dried beef	225
5.17	Chirped pulse THz images of dried beef	225
5.18	THz responses after transmission through beef and chicken samples	226

List of Figures

5.19	THz spectra of the responses shown in Fig. 5.18	226
5.20	Model output for second order FIR and AR filters	228
5.21	Scatter plot showing the discriminating power of the 2nd order FIR model coefficients	230
5.22	Scatter plot showing the distribution of the peak amplitude and the timing of the peak of the THz pulses for beef and chicken samples	230
5.23	Histogram of the 2nd order FIR model coefficients for the beef data	232
5.24	Histogram of the peak amplitude and the timing of the peak of the THz pulses	233
5.25	A standard optical image of a sample of dried chicken tissue	234
5.26	Terahertz images of the chicken tissue shown in Fig. 5.25	234
5.27	Photo of an envelope that contained <i>Bacillus anthracis</i> spores	236
5.28	THz image of 4 different powders and classification results	238
5.29	THz image of an envelope containing <i>Bacillus thuringiensis</i> spores	239
5.30	Photo of a teflon sample holder for powdered samples	240
5.31	Photo of the powder target	242
5.32	THz pulses after transmission through 2 mm of various powders	242
5.33	THz spectra after transmission through 2 mm of various powders	243
5.34	THz pulses after transmission through varying thickness of flour	243
5.35	THz spectra after transmission through varying thickness of flour	244
5.36	Scatterplot for powder data	245
5.37	Plot of maximum classifier accuracy as a function of the number of features	246
5.38	THz amplitude image of an envelope containing powders taped to form the characters 'THZ'	247
5.39	Classified image of an envelope containing powders taped to form the characters 'THZ'	248
5.40	Analysis of excised cancerous tissue using THz-TDS	253
5.41	Normal and cancerous cells viewed under a microscope	254
5.42	Scanned THz imaging system used to image cell flasks	255
5.43	THz pulses after transmission through the cells	256
5.44	THz amplitude spectra after transmission through the three flasks	256

5.45	Deconvolved THz amplitude spectra for the three flasks	257
5.46	Deconvolved THz phase spectra for the three flasks	257
5.47	Scatterplot of the THz amplitude at the optimum two frequencies	259
5.48	Scatterplot of the THz phase at the optimum two frequencies	260
5.49	Scatterplot of the THz amplitude at two random frequencies	261
5.50	Scatterplot of the THz phase at two random frequencies	262
5.51	Eigenvectors of the covariance matrix for the cellular THz responses . . .	263
5.52	Eigenvalues of the covariance matrix for the cellular THz responses . . .	263
5.53	Scatterplot of the projection of the THz responses onto the first two eigenvectors	264
5.54	Scatterplot of the projection of the THz responses onto the third and fourth eigenvectors	265

6.1	Schematic of holography target samples and their reconstructed holo- grams	273
6.2	A test structure imaged by the T-ray DT system and reconstructed result	274
6.3	Detailed polystyrene resolution test target and its reconstruction	276

B.1	Screenshot of the MFCPentamax software	290
B.2	Screenshot of the Labview tomography application	291

C.1	Sample geometry for a typical THz-TDS experiment	340
-----	--	-----

List of Tables

Table		Page
4.1	CT image parameters for the triangular test target	144
4.2	RMS error in τ for a number of peak estimator algorithms	150
4.3	T-ray CT imaging parameters for the 'THZ' polystyrene target	152
4.4	T-ray CT imaging parameters for the resolution test target	156
5.1	Examples of pattern recognition applications	185
5.2	Comparison of the major properties of wavelet bases	198
5.3	SNR of T-ray pulses after wavelet denoising	198
5.4	Experimentally determined ideal order for each wavelet family	199
5.5	Prediction accuracy for different models	229

